Available online at www.sciencedirect.com
SCIENCE DIRECT®
Journal of Molecular Catalysis A: Chemical 220 (2004) 247–255
JOURNAL OF MOLECULAR CATALYSIS A: CHEMICAL
www.elsevier.com/locate/molcata

Investigation of the effect of carbon monoxide on the oxidative carbonylation of methanol to dimethyl carbonate over Cu^+X and Cu^+ZSM-5 zeolites

Steven A. Anderson, Thatcher W. Root*

Department of Chemical and Biological Engineering, University of Wisconsin-Madison, 1415 Engineering Drive, Madison, WI 53706, USA

Received 2 July 2003; received in revised form 7 June 2004; accepted 8 June 2004

Abstract

Direct synthesis of dimethyl carbonate offers prospects for a "green chemistry" replacement to eliminate use of phosgene for polymer production and other processes. The carbonylation of methanol to produce dimethyl carbonate over Cu^+X and Cu^+ZSM-5 zeolites prepared by solid-state ion exchange has been investigated, focusing on the interaction of carbon monoxide with the Cu^+ zeolites. The methanol carbonylation mechanism reported previously has been extended to account for carbon monoxide adsorption at high pressure. The comparison of the results obtained from Cu^+X and Cu^+ZSM-5 show that strong CO adsorption on the catalyst is not related to increased rate of dimethyl carbonate production. The rate limiting step for DMC production is best described as the Eley-Rideal reaction of gas-phase CO with surface methoxide.

Keywords: Dimethyl carbonate; Methanol; Copper zeolites; Carbonylation

1. Introduction

Dimethyl carbonate (DMC) has been drawing attention from researchers due to its use in replacing environmentally unfriendly compounds [1]. The oxidative carbonylation of methanol has been pursued over a variety of copper catalysts as an "environment friendly," non-phosgene production pathway to DMC [2–9].

$$2\,CH_3OH + CO + \tfrac{1}{2}O_2 \rightarrow (CH_3O)_2CO + H_2O$$

Our previous findings extended the mechanistic understanding of the reaction pathway involved in the vapor-phase carbonylation of methanol to DMC over a Cu^+X zeolite catalyst, and described the surface reactions which lead to the formation of the by-products, methylal (MA) and methyl formate (MF) [10]. The results presented here enlarge the mechanism reported in our previous examination to include carbon monoxide adsorption onto the catalyst surface, which becomes important at high CO pressure.

The carbonylation mechanism over two copper zeolites, Cu^+X and Cu^+ZSM-5, has been studied. The Cu^+ZSM-5 adsorbs CO much more strongly than Cu^+X, and comparison of the catalysts has provided insight on the mechanistic nature of the interaction of CO with the species present on the catalyst surface under reaction conditions.

2. Experimental

2.1. Chemical reagents

The starting zeolite materials were an ammonium X zeolite with a Si/Al ratio of 1.4 (Aldrich) and an ammonium ZSM-5 zeolite with a Si/Al ratio of 14 (Zeolyst International). Reagents included cuprous chloride (>98%, Aldrich), methanol (A.C.S. grade, Fisher Scientific), oxygen (Medical Grade, Praxair), nitrogen (99.998%, Praxair), air (21% O_2/79% N_2, Praxair), and carbon monoxide (C.P. grade, Matheson).

* Corresponding author. Tel.: +1 608 262 8999; fax: +1 608 262 5434.
E-mail address: thatcher@engr.wisc.edu (T.W. Root).

1381-1169/$ – see front matter © 2004 Elsevier B.V. All rights reserved.
doi:10.1016/j.molcata.2004.06.006

2.2. Catalyst preparation

The copper zeolites were prepared by the solid-state ion exchange method, first described by Rabo et al. and Clearfield et al. [11–13]. King et al. found that Cu(I)/zeolites prepared by this method are excellent catalysts for the vapor-phase carbonylation of methanol to form DMC [8]. The solid-state ion exchange procedure involves mixing the zeolite powder (ammonium or acid form) and the exchange cation compound (usually a metal halide) and heating to a high temperature in vacuum or an inert atmosphere. The process results in the formation of the metal zeolite and the evolution of gases.

The Cu^+X zeolite catalyst was prepared by heating a physical mixture of 0.9 g CuCl and 1.1 g ammonium X zeolite in an argon stream at 625 °C for 16 h. The Cu^+ZSM-5 catalyst was made by heating a mixture of 0.22 g CuCl and 2.1 g ammonium ZSM-5 in a nitrogen stream at 625 °C for 16 h. Inductively coupled plasma (ICP) elemental analysis of the treated catalysts determined that the final copper content of Cu^+X and Cu^+ZSM-5 were 30 and 7 wt.%, corresponding to 96 and 100% of the full exchange capacity for each catalyst, respectively. Turnover frequencies were calculated based on the copper content of the catalysts.

2.3. Apparatus and operation

Kinetic studies of methanol carbonylation were conducted using a stainless-steel tubular reactor with a 5-mm inner diameter positioned in a temperature-controlled fluidized sand bath. In a typical run, 0.1–0.25 g of catalyst powder was packed into the reactor. Flow of nitrogen, oxygen, and carbon monoxide were controlled using mass flow controllers (MKS Instruments, Inc.). Methanol, water, and DMC flow rates were controlled by a syringe pump (Harvard Apparatus). The total gas flow rate to the reactor was typically 20 cm^3/min. The pressure of the system was controlled using a back pressure regulator (Grove Valve & Regulator Co.).

For liquid product analysis, the reactor effluent was passed through a cold trap kept at −117 °C and the liquid products were collected and analyzed using a Mattson Galaxy 5020 FT-IR spectrometer, typically using 256 scans with a resolution of 2 cm^{-1}. The IR cell used was a sealed liquid cell with CaF_2 windows and a path length of 0.05 mm, purchased from International Crystal Laboratories. After acquisition, spectra were deconvoluted into their components to quantify the reaction products.

2.4. In situ FTIR cell

All in situ FTIR spectra were obtained using an in situ FTIR cell as described by Yates and coworkers [14,15]. The cell was constructed within a standard stainless-steel tee having conflat flanges and commercial CaF_2 windows. The top port was sealed with a thermocouple/power feedthrough (Ceramaseal). To allow gas flow through the cell, two stainless-steel tubes were welded to the tee.

Flows of nitrogen, oxygen, and carbon monoxide were controlled using mass flow controllers (MKS Instruments, Inc.). The flow rates of methanol and water were controlled by flowing nitrogen or air through temperature-controlled bubblers. The in situ FTIR experiments were carried out at atmospheric pressure.

The spectra were taken using a Mattson Galaxy 5020 FT-IR spectrometer, typically using 128 scans with a resolution of 4 cm^{-1}. A background spectrum of the dry catalyst was taken prior to in situ experiments. After the reactant was introduced to the cell and a spectrum recorded, the dry catalyst spectrum was subtracted. IR spectra shown here display only the net spectral change of the surface of the catalyst.

3. Results

3.1. Reaction kinetics

Fig. 1 shows the effect of carbon monoxide pressure on the rates of production of DMC, MA, and MF over Cu^+X zeolite. Figs. 2 and 3 show the effect of methanol pressure on the methanol carbonylation rate over Cu^+X with a CO pressure of 0.4 and 2 atm, respectively. Fig. 4 shows the effect of CO pressure on the rates of production over Cu^+ZSM-5. Fig. 5 shows the effect of methanol pressure over Cu^+ZSM-5 when the CO pressure is 0.4 atm. Figs. 6 and 7 show the effect of oxygen and water pressure on the carbonylation rate over Cu^+ZSM-5. The lines in Figs. 1–7 show the rates of reaction over Cu^+X and Cu^+ZSM-5 predicted using the methanol carbonylation mechanism.

Table 1 lists the apparent power-law reaction orders for the rates of formation of DMC, MA, and MF with respect to carbon monoxide and methanol pressure determined from the data in Figs. 1–7. These power-law reaction orders are

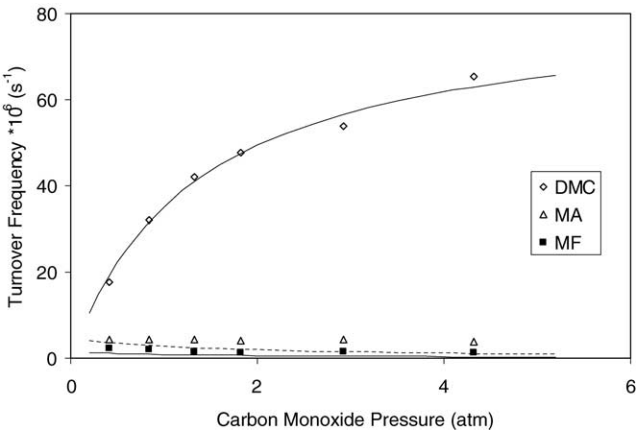

Fig. 1. Effect of carbon monoxide pressure on oxidative carbonylation of methanol over Cu^+X. Reaction conditions: reaction temperature 130 °C; methanol pressure 0.2 atm; oxygen pressure 0.08 atm.

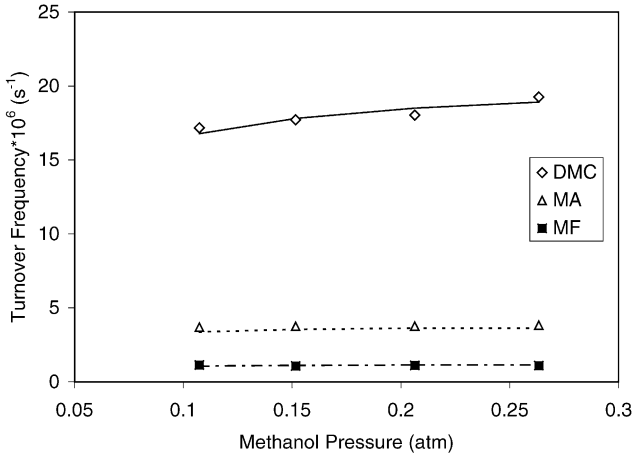

Fig. 2. Effect of methanol pressure on oxidative carbonylation of methanol over $Cu^{+}X$ zeolite. Reaction conditions: reaction temperature 130 °C; carbon monoxide pressure 0.4 atm; oxygen pressure 0.08 atm.

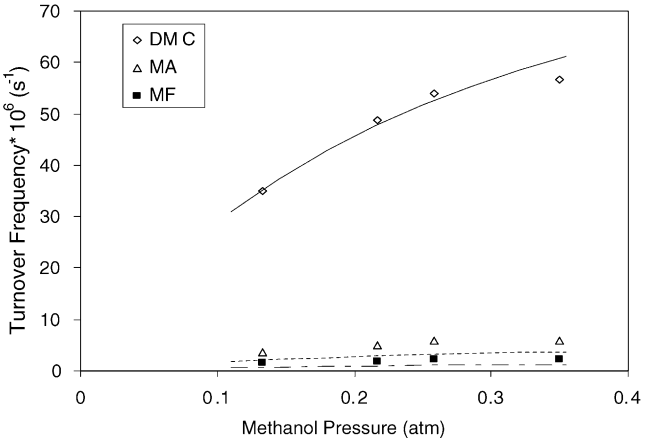

Fig. 3. Effect of methanol pressure on oxidative carbonylation of methanol over $Cu^{+}X$ zeolite. Reaction conditions: reaction temperature 130 °C; carbon monoxide pressure 2.0 atm; oxygen pressure 0.08 atm.

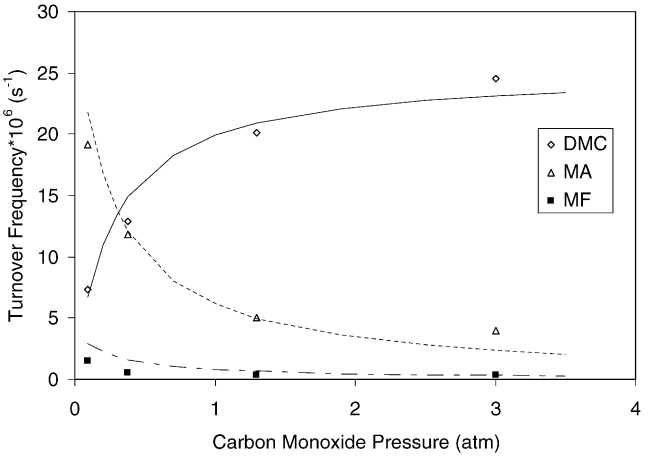

Fig. 4. Effect of carbon monoxide pressure on oxidative carbonylation of methanol over $Cu^{+}ZSM$-5. Reaction conditions: reaction temperature 130 °C; methanol pressure 0.2 atm; oxygen pressure 0.08 atm.

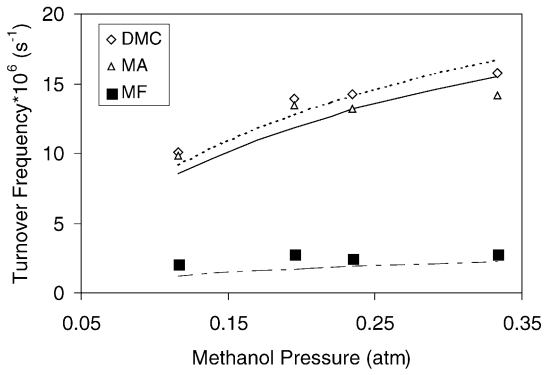

Fig. 5. Effect of methanol pressure on oxidative carbonylation of methanol over $Cu^{+}ZSM$-5. Reaction conditions: reaction temperature 130 °C; carbon monoxide pressure 0.3 atm; oxygen pressure 0.08 atm.

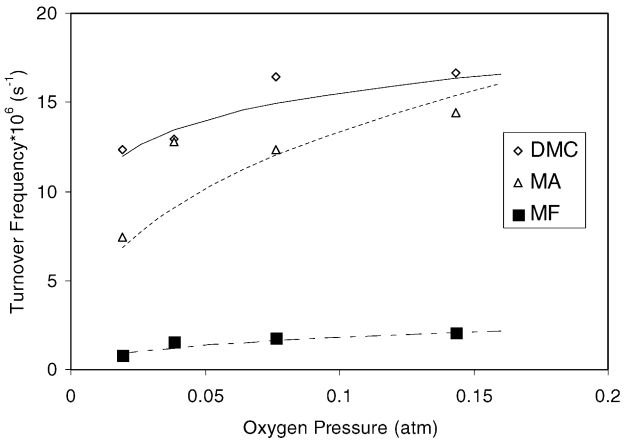

Fig. 6. Effect of oxygen pressure on oxidative carbonylation of methanol over $Cu^{+}ZSM$-5. Reaction conditions: reaction temperature 130 °C; carbon monoxide pressure 0.4 atm; methanol pressure 0.2 atm.

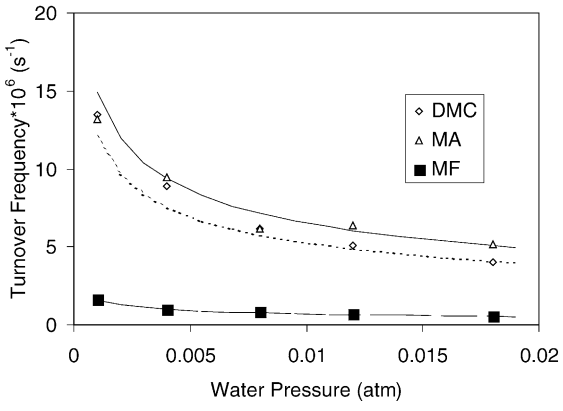

Fig. 7. Effect of water pressure on oxidative carbonylation of methanol over $Cu^{+}ZSM$-5. Reaction conditions: reaction temperature 130 °C; carbon monoxide pressure 0.4 atm; methanol pressure 0.2 atm; oxygen pressure 0.08 atm.

Table 1
Reaction orders for DMC, MA, and MF production

Catalyst	Reactant	Reaction orders		
		DMC	MA	MF
Cu^+X	Carbon monoxide	0.5	−0.1	−0.3
	Methanol (P_{CO} = 0.4 atm)	0.1	0	0
	Methanol (P_{CO} = 2.0 atm)	0.5	0.5	0.4
Cu^+ZSM-5	Carbon monoxide	0.4	−0.5	−0.4
	Methanol (P_{CO} = 0.4 atm)	0.4	0.3	0.3
	Oxygen	0.2	0.3	0.4
	Water	−0.5	−0.4	−0.4

convenient for characterizing reactor performance, and as a starting point for kinetic modeling.

3.2. In situ FTIR adsorption isotherm results

3.2.1. CO adsorption on Cu^+X zeolite

Equilibrium carbon monoxide adsorption on a fresh Cu^+X zeolite sample has been studied at two different carbon monoxide pressures, 0.11 and 0.022 atm, and a wide range of temperatures. For example, Fig. 8 shows how the intensity of the C–O stretching vibration (2140 cm^{-1}) of carbon monoxide adsorbed on Cu^+X varies with sample temperature under a constant CO pressure of 0.11 atm.

Under equilibrium conditions at a constant CO pressure, the Langmuir adsorption equilibrium expression can be rearranged to obtain the form

$$K_{eq} = \theta_{CO}/P_{CO}(1-\theta_{CO}) \quad (1)$$

with K_{eq} representing the equilibrium constant of adsorption, P_{CO} and θ_{CO} representing the gas phase pressure and surface coverage of carbon monoxide. The coverage of CO on the surface of the catalyst has been calculated from Eq. (2), using the Beer's Law approximation that the area under the IR peak is proportional to the amount of CO adsorbed on the catalyst surface,

$$\theta_{CO} = \frac{A_{CO}}{A_{CO}^{max}} \quad (2)$$

where A_{CO} is the area under the 2140 cm^{-1} peak and A_{CO}^{max} is the area corresponding to 100% coverage. A_{CO}^{max} was determined by fitting the data taken at the two pressures to Eq. (1) such as to minimize the difference in the calculated equilibrium constant at temperatures with multiple carbon monoxide pressures. Based on the fitted A_{CO}^{max}, the spectra recorded here correspond to CO coverages ranging from 1% $< \theta_{CO} <$ 94%. The points at extreme low and high temperature are less reliable because they are more sensitive to determination of the A_{CO}^{max} and to the baseline. In addition, any heterogeneity of site energetics would also cause deviations from linearity. The results reported here are averaged across all coverages and CO adsorption on copper is represented as a single species.

The enthalpy for CO adsorption on Cu^+X zeolite can be estimated from the Van't Hoff equation and the slope of $\ln K_{eq}$ plotted against $1/T$.

$$\Delta H_{ads} = R\frac{d(\ln K_{eq})}{d(1/T)} \quad (3)$$

ΔH_{ads} represents the enthalpy for adsorption and R is the gas constant. Fig. 9 shows the Van't Hoff plot for the adsorption of CO at two different pressures, illustrating the consistency of results from this approach. The heat of adsorption for carbon monoxide on the catalyst determined by this method is 64.7 ± 2.2 kJ/mol, and the equilibrium constant can be fit to $K_{eq}(T) = 1.6 \times 10^{-8} \exp(7780/T)\,atm^{-1}$. The heat of adsorption agrees well with the result of 62 kJ/mol of CO on Cu^+Y estimated using CO adsorption isotherms [16] and is in the range of 80–65 kJ/mol for carbon monoxide on Cu^+Y determined using microcalorimetry [17]. The pre-exponential factor agrees well with the estimated value of $5 \times 10^{-9}\,atm^{-1}$ calculated from Transition State Theory [18].

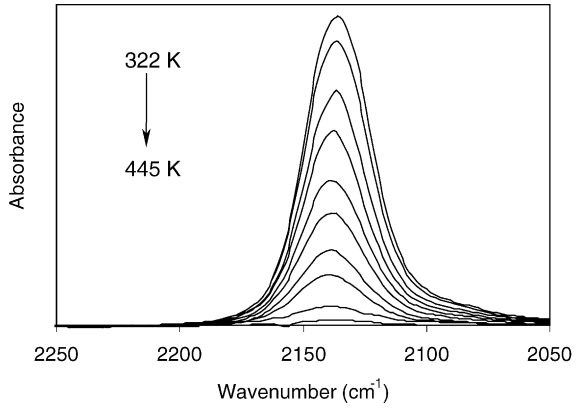

Fig. 8. Infrared spectra of carbon monoxide adsorption on Cu^+X showing the C–O stretching mode at 2140 cm^{-1}. CO pressure maintained at 0.11 atm.

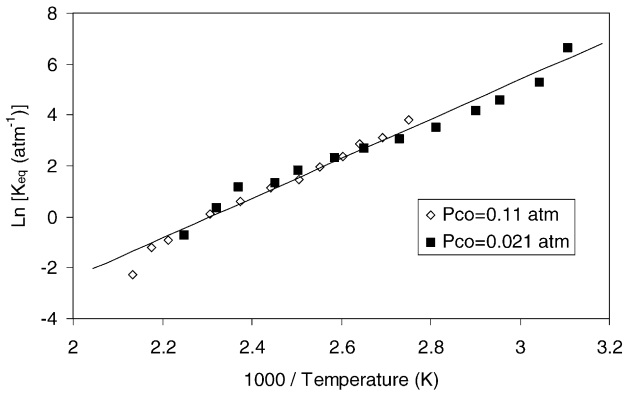

Fig. 9. Van't Hoff plot of carbon monoxide adsorption on Cu^+X zeolite.

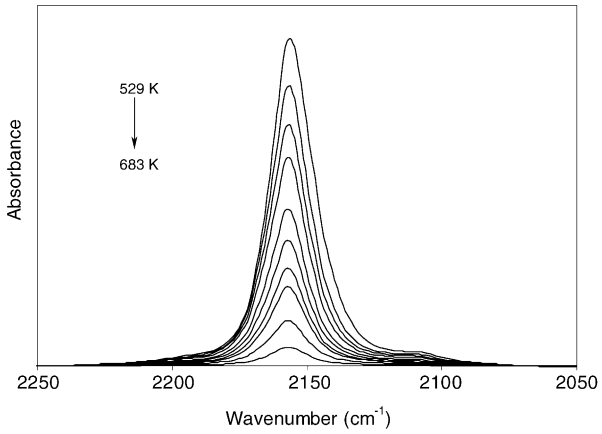

Fig. 10. Infrared spectra of carbon monoxide adsorption on Cu^+ZSM-5 showing the C–O stretching mode at 2157 cm^{-1}. CO pressure maintained at 0.014 atm.

3.3. CO adsorption on Cu^+ZSM-5 zeolite

Equilibrium carbon monoxide adsorption on a fresh Cu^+ZSM-5 sample has been studied at two different carbon monoxide pressures, 0.005 and 0.014 atm, and a wide range of temperatures. Fig. 10 shows the 2157 cm^{-1} C–O stretching vibration of carbon monoxide adsorbed onto Cu^+ZSM-5 at a CO pressure of 0.014 atm. The equilibrium constant for carbon monoxide adsorption on Cu^+ZSM-5 has been calculated using the same Langmuir adsorption equilibrium and Van't Hoff plot analysis (Fig. 11). The fitted A_{CO}^{max} for the Cu^+ZSM-5 catalyst indicates that these spectra correspond to CO coverages of $5\% < \theta_{CO} < 97\%$. The heat of adsorption for CO on Cu^+ZSM-5 is found to be 80.5 ± 3.5 kJ/mol, and the equilibrium constant can be fit to $K_{eq}(T) = 5.5 \times 10^{-6} \exp(9680/T)\,atm^{-1}$. This heat of adsorption is in the range of previous microcalorimetry investigations for CO on Cu^+ZSM-5, which determined heats of adsorption that vary from 91 to 70 kJ/mol [19], 120 to 100 kJ/mol [20], and 130 to 40 kJ/mol [21]. The pre-exponential factor is higher than the value estimated using Transition State Theory [18], which may account for the heat of adsorption measurement being on the low end of those reported in the literature.

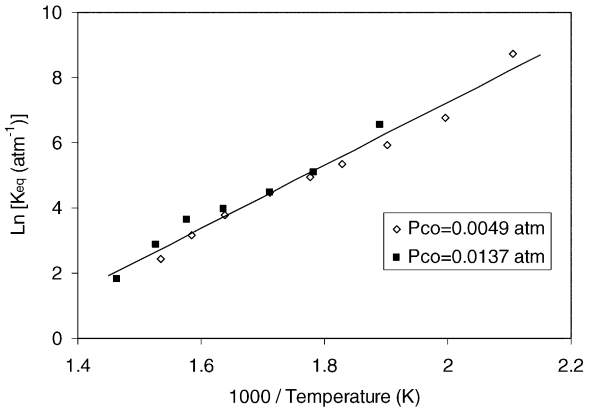

Fig. 11. Van't Hoff plot of carbon monoxide adsorption on Cu^+ZSM-5.

3.4. Methanol and water adsorption on Cu^+ZSM-5 zeolite

Equilibrium methanol and water adsorption experiments on a fresh Cu^+ZSM-5 sample have been studied using in situ FTIR spectroscopy at different pressures and temperatures. The strength of adsorption for methanol and water on Cu^+ZSM-5 were found to be similar to that of these species on Cu^+X [10]. The values for the equilibrium constants for methanol and water adsorption on Cu^+ZSM-5 at 130 °C are shown in Table 2.

3.5. Surface species under reaction conditions

Carbon monoxide, methanol, and oxygen adsorption on Cu^+X and Cu^+ZSM-5 have been studied at 130 °C to allow investigation of the surface species present under reaction conditions. The catalyst was exposed to an atmosphere containing methanol, oxygen, and carbon monoxide, and the gas composition and temperature were kept constant for 30 min to allow the surface to equilibrate. After equilibration, the cell was purged with nitrogen at a flow rate of 2000 cm^3/min and spectra were taken with the catalyst surface maintained at 130 °C. Fig. 12 shows the surface species present on the surface of the Cu^+X and Cu^+ZSM-5 immediately after purging the cell of gas phase species. The carbon monoxide stretching frequency occurs at 2140 cm^{-1} for Cu^+X and at 2137 and 2157 cm^{-1} for Cu^+ZSM-5. The adsorption bands in the methanol/methoxide region (1340–1540 cm^{-1}) are located at similar wavenumbers for both catalysts.

4. Mechanism

In our previous paper, we presented a detailed mechanism for the oxidative carbonylation of methanol over a Cu^+X zeolite catalyst [10]. The * represents the active site (Cu^+Ze^-). Here we have included the adsorption of CO onto Cu^+Ze^- (step R11) to describe the coverage of CO at the higher pressures of this study.

$$CH_3OH + * \leftrightarrow CH_3OH* \quad (R1)$$

$$CH_3OH* + \tfrac{1}{4}O_2 \leftrightarrow CH_3O* + \tfrac{1}{2}H_2O \quad (R2)$$

$$CH_3O* + CO \leftrightarrow CH_3OCO* \quad (R3)$$

$$CH_3OCO* + CH_3O* \leftrightarrow (CH_3O)_2CO + 2* \quad (R4)$$

$$CH_3O* + \tfrac{1}{4}O_2 \leftrightarrow CH_2O* + \tfrac{1}{2}H_2O \quad (R5)$$

$$CH_2O* \leftrightarrow CH_2O + * \quad (R6)$$

$$CH_2O + 2\,CH_3OH \leftrightarrow (CH_3O)_2CH_2 + H_2O \quad (R7)$$

$$CH_2O + \tfrac{1}{2}O_2 \leftrightarrow HCOOH \quad (R8)$$

Table 2
Parameters for the oxidative carbonylation mechanism over Cu^+X and Cu^+ZSM-5 at 130 °C

Catalyst	Parameter	Value and units	Reference
Cu^+X	k_3	$(7.35 \pm 0.61) \times 10^{-5}$ atm^{-1} s^{-1}	12
	K_1	11.57 atm^{-1}	12
	K_2	0.102 ± 0.021 atm$^{0.25}$	12
	K_{10}	84.6 atm^{-1}	12
	K_{11}	3.9 atm^{-1}	This work (FTIR)
	k_5	$(1.36 \pm 0.04) \times 10^{-5}$ atm$^{-0.25}$ s^{-1}	12
	ϕ_{MA}	0.760 ± 0.016	12
Cu^+ZSM-5	k_3	$(9.64 \pm 2.02) \times 10^{-5}$ atm^{-1} s^{-1}	This work (kinetic fit)
	K_1	11.6 atm^{-1}	This work (FTIR)
	K_2	863 ± 260 atm$^{0.25}$	This work (kinetic fit)
	K_{10}	83.1 atm^{-1}	This work (FTIR)
	K_{11}	1.5×10^5 atm^{-1}	This work (FTIR)
	k_5	$(6.41 \pm 0.38) \times 10^{-5}$ atm$^{-0.25}$ s^{-1}	This work (kinetic fit)
	ϕ_{MA}	0.882 ± 0.018	This work (kinetic fit)

$$CHOOH + CH_3OH \leftrightarrow CHOOCH_3 + H_2O \quad (R9)$$

$$H_2O + * \leftrightarrow H_2O* \quad (R10)$$

$$CO + * \leftrightarrow CO* \quad (R11)$$

Steps R1 through R4 provide the basic mechanism for DMC formation. The first step of the mechanism is the adsorption of methanol onto a copper site of the zeolite. The second step of this mechanism is a sum of several rapid, equilibrated steps that result in the formation of methoxide. Methanol adsorption on the active site of the catalyst has been shown in previous examinations [9,10], and the effect of oxygen and water on the equilibrium of the surface methoxide formed in step 2 has been well described [10].

The third step is the Eley-Rideal insertion of carbon monoxide to form carbomethoxide, which is rate limiting for DMC production. In the fourth step the carbomethoxide reacts rapidly with additional methoxide to form DMC. Experimental evidence of the interaction of CO with surface methoxide has been shown previously [9].

Steps R5 through R9 provide for formation of the two major by-products. The key intermediate in the formation of methylal and methyl formate is the formaldehyde produced by the oxidation of surface methoxide. The oxidation of surface methoxide is the rate-limiting step for formaldehyde formation. The formaldehyde formed reacts quickly with abundant methanol to form the by-products, no formaldehyde is detected in the reactor effluent. The reaction steps that produce methylal and methyl formate from formaldehyde have been shown to occur via steps R7–R9 [10]. The sites that catalyze these steps are not fully understood, but methylal appears to be generated over H^+ sites and methyl formate over Cu^0 sites. It has been shown that copper zeolite catalysts prepared by the solid-state ion exchange method have residual H^+ sites, due to incomplete exchange of the H^+ sites with Cu^+ ions during catalyst preparation [22]. Also, Li et al. have shown that the SSIE method produces some Cu^0 species due to the reaction of copper with the silanol groups, forming Si–O–Cu species [23]. Turnover frequencies are based on the copper content of the catalyst, although it is not expected that all copper exists as Cu^+ species.

Water significantly decreases the reaction rates over the copper zeolite catalysts, both by its effect on the equilibrium

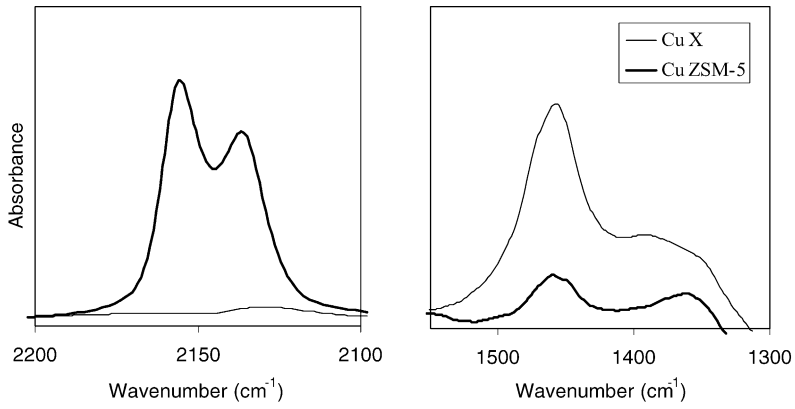

Fig. 12. Infrared spectra of adsorbed species on Cu^+X and Cu^+ZSM-5 showing C–O stretching region (2100–2200 cm^{-1}) and the δ_{CH} mode of methanol and methoxide.

of methoxide formation (step 2) and also by adsorption onto the Cu^+ sites (step R10). Water is produced in steps R2, R7, and R9 of the reaction mechanism, so water will always be present as the reaction proceeds.

Carbon monoxide adsorption on the catalyst surface (step R11) is an additional site-blocking step that prevents the formation of methoxide on the active sites. Because the CO insertion into the methoxide species to form a carbomethoxide species occurs via an Eley-Rideal pathway, carbon monoxide adsorption onto Cu^+Ze^- has a negative influence on the rate of DMC production because of this competition for sites. The following paragraphs extend our earlier model to include the effect of competitive adsorption of non-reactive CO.

The rates of formation of DMC and the two by-products are described by Eqs. (4)–(6) shown below, which are the result of treating step R3 as the rate-limiting step for DMC production and R5 being the rate-limiting step by-product formation, and steps R1, R2, R10, and R11 being equilibrated

$$R_{DMC} = k_3 P_{CO} \theta_{CH_3O} \tag{4}$$

$$R_{MA} = \phi_{MA} R_{Form} = \phi_{MA} k_5 P_{O_2}^{1/4} \theta_{CH_3O} \tag{5}$$

$$R_{MF} = \phi_{MF} R_{Form} = \phi_{MF} k_5 P_{O_2}^{1/4} \theta_{CH_3O} \tag{6}$$

R_{DMC}, R_{MF}, R_{MA}, and R_{Form} represent the rates of formation of DMC, MF, MA, and formaldehyde, k_3 and k_5 are the rate constants for the forward reactions of step R3 and R5, θ_{CH_3O} is the fraction of methoxide sites on the catalyst surface, and the coefficients ϕ_{MA} and ϕ_{MF} and the relative amounts of methylal and methyl formate formed from the formaldehyde produced, with $\phi_{MA} = r_7/(r_7 + r_8)$ and $\phi_{MF} = r_8/(r_7 + r_8)$, where r_7 and r_8 are the rates of steps R7 and R8, respectively. The reverse reactions for the slow steps may be neglected both because of the low conversion and the thermodynamic equilibrium of the overall reactions highly favoring the formation of products under the reaction conditions.

The four most abundant surface intermediates are adsorbed methanol, surface methoxide, adsorbed water, and adsorbed carbon monoxide. The coverages of carbomethoxide and adsorbed DMC are insignificant under these conditions [9]. Therefore, θ_* can be determined from Eq. (7).

$$\begin{aligned}\theta_* &= 1 - (\theta_{CH_3OH} + \theta_{CH_3O} + \theta_{H_2O} + \theta_{CO}) \\ &= \left[1 + K_1 P_{MeOH} + \frac{K_1 K_2 P_{MeOH} P_{O_2}^{1/4}}{P_{H_2O}^{1/2}} + K_{10} P_{H_2O} + K_{11} P_{CO}\right]^{-1}\end{aligned} \tag{7}$$

The combination of the equations which describe the surface species with Eqs. (4)–(6) provide expressions for the rates of formation of DMC, MA, and MF.

$$R_{DMC} = \frac{k_3 K_1 K_2 P_{MeOH} P_{CO} P_{O_2}^{1/4} / P_{H_2O}^{1/2}}{[1 + K_1 P_{MeOH} + K_1 K_2 P_{MeOH} P_{O_2}^{1/4} / P_{H_2O}^{1/2} + K_{10} P_{H_2O} + K_{11} P_{CO}]} \tag{8}$$

$$R_{MA} = \frac{\phi_{MA} k_5 K_1 K_2 P_{MeOH} P_{O_2}^{1/2} / P_{H_2O}^{1/2}}{[1 + K_1 P_{MeOH} + K_1 K_2 P_{MeOH} P_{O_2}^{1/4} / P_{H_2O}^{1/2} + K_{10} P_{H_2O} + K_{11} P_{CO}]} \tag{9}$$

$$R_{MF} = \frac{\phi_{MF} k_5 K_1 K_2 P_{MeOH} P_{O_2}^{1/2} / P_{H_2O}^{1/2}}{[1 + K_1 P_{MeOH} + K_1 K_2 P_{MeOH} P_{O_2}^{1/4} / P_{H_2O}^{1/2} + K_{10} P_{H_2O} + K_{11} P_{CO}]} \tag{10}$$

The values for K_1, K_2, k_3, k_5, K_{10}, and ϕ_{MA} over Cu^+X are as determined in our previous investigation [10]. The predicted rates for the carbonylation of methanol over Cu^+X zeolite shown in the Figs. 1–3 are obtained by using the fitted parameters from the previous study and adding the K_{11} adsorption constant for CO on Cu^+X zeolite, modeling the reactor as a plug flow reactor. No adjustment of these parameters was necessary to obtain the fits to the data in Figs. 1–3.

The values for the kinetic parameters (K_2, k_3, k_5, and ϕ_{MA}) for the Cu^+ZSM-5 catalyst were determined using Athena Visual Workbench [24]. This software employs a general regression analysis of the kinetic data with the reactor modeled as a continuous stirred-tank reactor. The analysis used an average reactor water pressure based on the feed water pressure and half the contribution of water generated by the measured overall reaction rates of all products, which varied slightly with methanol conversion and reaction selectivity. The values for methanol, water, and carbon monoxide adsorption (K_1, K_{10}, and K_{11}) have been determined using in situ FTIR spectroscopy, and were not adjusted during the general regression analysis. The lines shown in Figs. 4–7 show the rates of reaction predicted using the rate expressions for DMC, MA, and MF and the fitted parameters listed in Table 2 for the Cu^+ZSM-5 catalyst.

5. Discussion

The nature of the copper site formed from the interaction of CuCl with H^+Y and H^+ZSM-5 during the solid-state ion exchange procedure has been the subject of previous examinations [22,23]. Exact characterization of the catalyst has not been a focal point of this investigation, and the turnover frequencies are based on the copper content of the catalyst determined from elemental analysis of the sample.

Cu^+X is the preferred catalyst over Cu^+ZSM-5 for the oxidative carbonylation of methanol to DMC for two reasons. The copper sites of Cu^+X show higher activity and selectivity for DMC production than Cu^+ZSM-5, and the zeolite framework of X has a higher aluminum content than

ZSM-5, which allows for more Cu^+ sites per gram of catalyst.

The reaction order for DMC production with respect to carbon monoxide pressure decreases below unity as the CO pressure increases over Cu^+X zeolite. Carbon monoxide adsorption on the catalyst surface is the cause of this decrease in reaction order, shown by the accuracy of the predicted rates shown in Fig. 1 calculated using the rate expressions and the parameters in Table 2. The rates of production of MA and MF both decrease with increasing carbon monoxide pressure, which is further indication that CO adsorption on the catalyst surface decreases the coverage of methoxide on the surface. The decrease of the by-product formation rate is even more apparent over Cu^+ZSM-5 (Fig. 4). As a result of this site competition by non-reactive CO, it is clear that the rate and selectivity improvements obtained by increasing CO pressure at low pressure will pass through an optimum, and it is expected that sufficiently high CO pressure will result in constant or reduced DMC production rates for both copper zeolite catalysts.

The reaction order with respect to methanol pressure for DMC production over Cu^+X increases from 0.1 at a CO pressure of 0.4 atm to 0.5 at a CO pressure of 2.0 atm. This indicates that methanol and methoxide dominate the surface at low CO pressure and cover less of the surface as the CO pressure increases, caused by both species competing to adsorb on the same copper site. Carbon monoxide adsorption is stronger on Cu^+ZSM-5 than on Cu^+X, and the reaction order for DMC production with respect to methanol is higher over Cu^+ZSM-5 than over Cu^+X for a carbon monoxide pressure of 0.4 atm. In the in situ FTIR spectra of both catalysts under reaction conditions (Fig. 12), the Cu^+ZSM-5 shows a much higher ratio of CO coverage/methoxide coverage than Cu^+X, which agrees qualitatively with the surface coverage of CO predicted by the modeling of the kinetic experiments. It is difficult to obtain a quantitative measurement for these ratios, because the Cu^+ZSM-5 shows a strong peak at 2137 cm^{-1}, which has been observed previously as CO adsorption on a weaker Cu^+ site [19].

Carbon monoxide absorbs on the same catalyst site as methanol, as has been reported previously [9]. This is the cause for the decrease in reaction order for DMC production with increasing CO pressure, and the negative reaction orders for by-product formation with respect to CO pressure. If CO adsorption occurred on a different site, a negative reaction order for by-product formation would not be observed, counter to what is seen experimentally. Also, CO adsorption occurring on a different site would result in CO pressure having no effect on the reaction rate order for DMC with respect to methanol pressure, which is counter to experimental observation.

The reaction orders for DMC production with respect to methanol and carbon monoxide support the rate-limiting, Eley-Rideal reaction of CO with the surface methoxide species. If surface methoxide reacted with an adsorbed CO species, the reaction rates predicted with the mechanism would contain a squared denominator. Thus, reaction with an adsorbed CO species would result in a negative reaction order with respect to methanol pressure when methoxide coverage dominates the catalyst surface, which is not seen experimentally. Also, the reaction order with respect to CO pressure would become negative at high pressure, which is not seen over Cu^+X nor the strongly CO absorbing Cu^+ZSM-5 catalyst.

6. Conclusions

Cu^+X has been shown to be a better catalyst than Cu^+ZSM-5 for DMC production. The weaker adsorption of CO onto Cu^+X compared to Cu^+ZSM-5 is advantageous for DMC production because adsorbed CO blocks sites for methoxide formation but does not participate in DMC formation. The rate-determining step for DMC production is insertion of gaseous carbon monoxide into surface methoxide to form a carbomethoxide, via an Eley-Rideal pathway. This competition between direct adsorption of non-reactive CO and Eley-Rideal reaction of CO with the surface methoxide will result in decreasing benefits for DMC production at high CO pressures.

Acknowledgements

We gratefully acknowledge the financial support of the National Science Foundation Training Grant for the program “Catalysis for Environmentally Conscious Manufacturing” (DGE-9554586). We thank Mr. S. Manthata for his efforts involving the collection of kinetic data over the Cu^+ZSM-5 catalyst.

References

[1] Y. Ono, Appl. Catal. A: Gen. 155 (1997) 133.
[2] U. Romano, R. Tesel, M.M. Mauri, P. Rebora, Ind. Eng. Chem. Prod. Res. Dev. 19 (1980) 396.
[3] U. Romano, Chim. Ind. 75 (4) (1993) 303.
[4] G.L. Curnutt, U.S. Patent 5004827, 1991.
[5] K. Tomishige, T. Sakaihori, S. Sakai, K. Fujimoto, Appl. Catal. A: Gen. 181 (1999) 95.
[6] M. Zinbin, Z. Renzhe, X. Genhui, H. Fei, C. Hongfang, Catal. Today 30 (1996) 201.
[7] Y.J. Wang, Y.Q. Zhao, B.G. Yuan, B.C. Zhang, J.S. Cong, Appl. Catal. A: Gen. 171 (2) (1998) 255.
[8] S.T. King, M.E. Jones, M.M. Olken, U.S. Patent 5391803, 1995.
[9] S.T. King, J. Catal. 161 (1996) 530.
[10] S.A. Anderson, T.W. Root, J. Catal. 217 (2003) 396.
[11] J.A. Rabo, M.L. Poutsma, G.W. Skeels, in: J.W. Hightower (Ed.), Proceedings of the Fifth International Congress on Catalysis, Palm Beach 1972, North Holland, Amsterdam, 1973, p. 1353.
[12] J.A. Rabo, Zeolite chemistry and catalysis ACS monograph, Am. Chem. Soc. Washington DC 171 (1976) 332.
[13] A. Clearfield, C.H. Saldarriaga, R.C. Buckley, in: J.B. Uytterhoeven (Ed.), Proceedings of Third International Congress on Molecular Sieves, Zurich, University of Leuven Press, 1973, p. 241.

[14] T.H. Ballinger, J.C.S. Wong, J.T. Yates Jr., Langmuir 8 (1992) 1676.
[15] T.P. Beebe, P. Gelin, J.T. Yates Jr., Surface Sci. 148 (2/3) (1984) 526.
[16] Y.Y. Huang, J. Catal. 30 (1973) 187.
[17] G.D. Borgard, S. Molvik, P. Balaraman, T.W. Root, J.A. Dumesic, Langmuir 11 (6) (1995) 2065.
[18] R.D. Cortright, J.A. Dumesic, Adv. Catal. 46 (2001) 161.
[19] Y. Kuroda, Y. Yoshikawa, R. Kumashiro, M. Nagao, J. Phys. Chem. B 101 (1997) 6497.
[20] R. Kumashiro, Y. Kuroda, M. Nagao, J. Phys. Chem. B 103 (1999) 89.
[21] V. Bolis, S. Maggiorini, L. Meda, F. D'Acapito, G. Turnes Palomino, S. Bordiga, C. Lamberti, J. Chem. Phys. 113 (20) (2000) 9248.
[22] H.G. Karge, B. Wichterlova, H.K. Beyer, J. Chem. Soc. Faraday Trans. 88 (9) (1992) 1345.
[23] Z. Li, K. Xie, R.C.T. Slade, Appl. Catal. A: Gen. 209 (2001) 107.
[24] M.C. Caracotsios, W.E. Stewart, Athena Visual Workbench 8.2, Stewart and Associates, Madison, WI, 2002.